Urko de la Torre[a], Jacques Lacaze[b], Jon Sertucha[a]
[a]Ingeniaritza, I+G eta Metalurgi Prozesuak, IK4-AZTERLAN, Durango (Bizkaia), Spain
[b]CIRIMAT, Université de Toulouse, Toulouse, France

Chunky graphite formation in ductile cast irons: effect of silicon, carbon and rare earths

Use of rare earths, high silicon and carbon contents, and low cooling rates are reported as possible reasons for formation of chunky graphite in ductile iron castings. The understanding of this graphite degeneration is however limited, and the above conclusions are still controversial. To get further insight into this topic, ductile cast iron melts have been prepared with various carbon and silicon contents and using nodularizing alloys with various rare earth levels. These melts have been cast in blocks with different sizes to include also the effect of cooling rate on graphite degeneration. Metallographic investigation revealed that the chunky-affected areas enlarge when decreasing the cooling rate, when increasing the silicon content and without low-level addition of rare earth. In the discussion, a schematic based on change of liquid/graphite interfacial energy with alloying elements is proposed which describes the conditions for the formation of chunky graphite instead of nodular graphite.

Keywords: Ductile cast iron; Heavy section casting; Chunky graphite; Rare earth; Silicon

1. Introduction

Degeneration of the spherical shape of graphite precipitates in ductile cast irons is one important concern faced by foundries, in particular in the case of heavy section components. Historically, both magnesium and cerium – and more generally rare earth (RE) – have been demonstrated to be graphite nodularizers when added at quite low level (typically 0.03–0.1 mass%). Magnesium is preferred however because it is much cheaper and more efficient than RE as mentioned long ago by White et al. [1]. These authors have compared the nodularizing capability of magnesium and cerium by casting Y-blocks $^1/_4$, $^1/_2$, 1 and 3 inches in section size with increasing amounts of either magnesium or cerium. Their results are reproduced in Fig. 1 where it is seen that a residual magnesium content higher than 0.040 mass% ensures optimum nodularity, though this latter decreases slightly with section size. The nodularizing effect of cerium is limited to an optimum value around 0.055 mass% with a maximum nodularity that is highly sensitive to section size. While the improvement of nodularity up to the optimum value is associated with the deoxidizing and desulfurizing action of either magnesium or cerium, Fig. 1 shows also that addition of cerium above 0.055 mass% leads to graphite degeneration. Similarly, overtreatment with magnesium leading to degeneration of graphite has also been reported [2, 3] though at higher residual magnesium content than shown in Fig. 1. Considering Fig. 1, it may be understood that it has become usual practice to add small quantities of cerium or RE in association with magnesium to improve nodularity as cerium is a much more potent deoxidizer than magnesium.

However, too high additions of RE could be detrimental, and this has been claimed to be one of the possible reasons for nodular graphite degeneracy known as chunky graphite [4, 5]. Chunky graphite consists of interconnected strings of graphite [6–8] and often appears as rounded cells very much like coral graphite. The difference between these two forms being that the overall or apparent graphite growth direction is along the basal ***c*** axis for chunky and along the prismatic ***a*** axis for coral graphite, see for example the review by Lacaze et al. [8]. As does coral graphite, chunky graphite results from a coupled growth of austenite and graphite and it has been suggested it appears at quite low eutectic undercooling [8].

Silicon has also been reported as promoting chunky graphite and Karsay and Campomanes [9] proposed a maximum silicon content as function of section size. The corre-

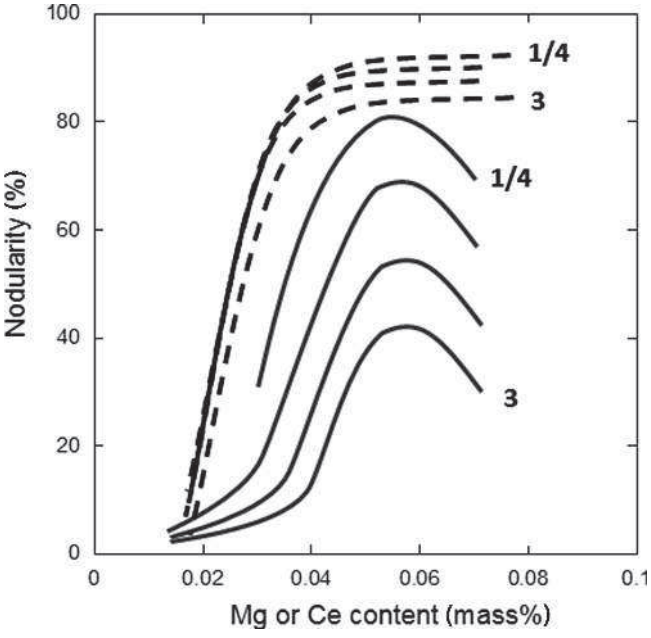

Fig. 1. Effect of magnesium (dashed lines) and cerium (solid lines) on nodularity for various sections sizes, $^1/_4$, $^1/_2$, 1 and 3 inches. After White et al. [1].

lation between solidification time (section size) and silicon content has been further studied, though the reported critical level certainly depends on impurities present in the alloy [10 – 12]. Attempts have been made recently to quantify the possible effect of some of the most powerful impurities and low level elements [13, 14]. The effect of silicon as being due to an increase in carbon equivalent has since long been disregarded [9] though it would be in line with the proposal by Gagné and Argo [15] that chunky graphite is due to high carbon supersaturation of the melt.

The present study was dedicated to gain some further insight into the respective effects of silicon and rare earths (RE) on chunky graphite formation. Three sets of alloys with various silicon and carbon contents have been prepared using various nodularizers and inoculants. Further, these alloys were cast in Y-blocks of different sizes so as to include the effect of cooling rate.

2. Experimental details

The melts were prepared in a medium frequency induction furnace (250 Hz, 100 kW) of 100 kg in capacity from metallic charges composed of low-alloyed steel scrap, returns of a low alloyed ferritic cast iron, high purity graphite (mass% C > 99.0) and an FeSi alloy (mass%, Si = 74.6, C = 0.12, Al = 0.83 and balance Fe). After melting, the composition of the melts was checked and carbon and silicon contents were then adjusted according to the defined targets. The transfer of the melt from the furnace to a 70 kg capacity ladle was made at a temperature between 1 500 °C and 1 520 °C. The nodularizing treatment was carried out following the sandwich method adding an RE-free (NRE in the following) or an RE-bearing (RE in the following) FeSiMg alloy. The nodularizer was added at an amount of 1.5 % (without rare earths) and 1.2 % (with rare earths) of the total weight of the ductile iron alloy. Once the nodularizing reaction had finished, the melt was skimmed and a sample was taken out for checking the final composition of the alloy.

Inoculation was performed in mold with an FeSi alloy added at a level 0.2 % of the total weight of the ductile iron alloy poured in the mold. One FeSi alloy without RE (denoted FE in the following) and one containing traces of RE (denoted FERE in the following) were used. The RE-free inoculant was used for batches treated using FeSiMg with (RE) and without (NRE) rare earth, while the inoculant containing traces of RE was used only on batches treated with the RE-bearing FeSiMg. The compositions of the nodularizers and inoculants used in the present work are listed in Table 1.

The castings were Y2, Y3 and Y4 keel-blocks (as per standard EN 1563) and a staircase casting with four steps of 8, 18, 32 and 63 mm high (see Fig. 2). Only the keel-blocks were used in this study. Three types of alloy compositions were considered: low-silicon eutectic alloys (LSi), high-silicon eutectic alloys (HSi) and high-silicon hypereutectic alloys (HSiHC). For each chemical composition, three molds were poured with melts corresponding to: 1) both nodularization and inoculation without RE (NRE-FE); 2) nodularization with RE and inoculation without RE (RE-FE); and 3) both nodularizer and inoculant containing RE (RE-FERE). This means in total nine molds.

After cooling, all castings were removed from the layout and then cleaned. Y4 keel-blocks were cut longitudinally to obtain the largest symmetric section while Y3 and Y2 keel-blocks were cut transversally. Macroscopic inspection was carried out on all sections to delimit the areas affected by chunky graphite (CHG) which commonly appear with a darker contrast in the internal part of the castings. A macrograph of each section was then taken and the area affected by chunky graphite was estimated by means of the image analysis software ImageJ. Additional metallographic inspection was carried out in those cases in which the area containing chunky graphite did not show high enough contrast to securely define its boundaries. The fraction of the section surface affected by chunky graphite, f_{CHG}, was finally determined as $S_{CHG} \cdot 100/S_{section}$, where S_{CHG} and $S_{section}$ are the area affected by chunky graphite and the total area of the section respectively. Finally, effectiveness of inoculation was evaluated by measuring the nodule count at the bottom of Y2 keel-blocks which was always free of CHG.

The chemical composition of the castings was determined on samples machined out from one of the keel-blocks produced in each mold. One part of these samples

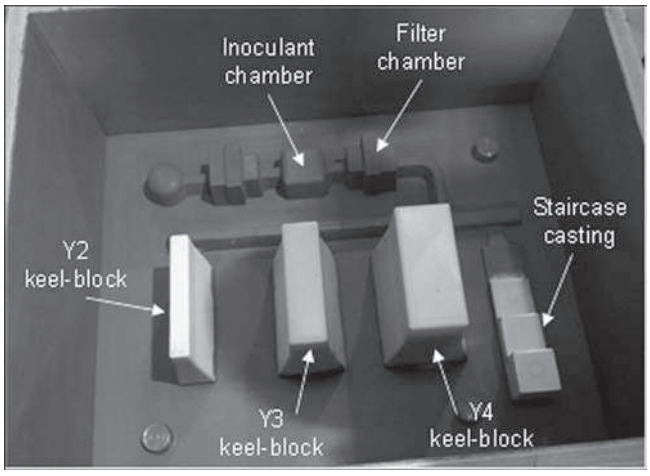

Fig. 2. Pattern used for preparing the poured castings.

Table 1. Composition of the nodularizers and of the inoculants (mass%), balance Fe.

Ferroalloy	Code	Mg	Ca	Al	RE	Ce	La	C	Si
FeSiMg	NRE	6.26	0.83	0.25		<0.05	0.16		43.2
	RE	6.47	0.98	0.67	0.97				46.2
Inoculant	FE			0.83				0.12	74.6
	FERE	traces	0.3 – 1.5	3.2 – 4.5	traces				68 – 76

was used for determining carbon and sulfur contents using combustion analysis (LECO CS300). The other part was dissolved in acid and the resulting solution was analyzed using the inductive coupled plasma – mass spectroscopy (ICP–MS) technique with an Agilent 7500ce facility to determine the content of other elements.

3. Results

The chemical compositions of the alloys as measured on the keel-blocks are listed in Table 2. The content of some minor elements appeared sometimes lower than the established detection limit. In such a case, the detection limit is reported preceded by a lower (<) sign. In all cases, Mo, Bi, Pb and Sn were also analyzed and found below their detection limit at 0.02, 0.0005, 0.0005 and 0.0005 mass% respectively. In Table 2 are also reported two values of carbon equivalent *CE*, denoted *CE** and *CE*** and calculated respectively following Castro et al. [16] and the ASM handbook [17]:

$$CE^{*} = \%C + 0.28 \cdot \%Si + 0.007 \cdot \%Mn + 0.092 \cdot \%Cu + 0.303 \cdot \%P$$

$$CE^{**} = \%C + 0.31 \cdot \%Si - 0.027 \cdot \%Mn + 0.076 \cdot \%Cu + 0.33 \cdot \%P + 0.4 \cdot \%S$$

For determining if an alloy is hypo- or hyper-eutectic, *CE** should be compared to 4.34 and *CE*** to 4.30. It is thus seen that LSi alloys are slightly hypo-eutectic, HSi alloys would be either slightly hypo- or slightly hyper-eutectic depending on the *CE* used, and HSiHC alloys are hyper-eutectic as expected from their carbon and silicon contents.

Typical micrographs taken on the Y4 blocks are shown in Fig. 3. In both LSi alloys containing RE (LSi-RE-FE and LSi-RE-FERE), a nearly fully nodular structure was observed with very little degenerate graphite precipitates and no chunky graphite. In contrast, alloy LSi-NRE-FE without RE showed chunky graphite which appears as large rounded cells that should have formed early during the bulk eutectic reaction. In all HSi alloys, chunky graphite has developed to such a large extent that the individual cells have impinged on each other and cannot be distinguished. In many cases, austenite dendrites with large nodules trapped in are clearly delineated by chunky graphite, suggesting that solidification of HSi alloys started by nucleation of a few nodules growing into the liquid which then get encapsulated into austenite dendrites at the very start of the eutectic reaction. After some while, the temperature and the composition of the liquid are such that bulk eutectic solidification can take place which proceeds by first giving chunky graphite. Chunky cells do not generally fill all the available space and solidification ends with nucleation and eutectic growth of small-size secondary nodules.

Figure 4 shows an example of the section of a Y3 keel-block where the contrast change associated with formation of chunky graphite can be easily seen. The values of the fraction of the surface section affected by chunky (f_{CHG}) for all castings are listed in Table 3 and reported in Fig. 5. Focusing first on the effect of casting size, it is seen that increasing the cooling rate from Y4 to Y2 decreases the amount of chunky graphite as expected from literature [18–20]. Note that the beneficial effect of higher cooling rate seems to be more pronounced from Y3 to Y2 than from Y4 to Y3.

The negative effect of silicon on casting quality reported in the literature [9, 10, 12] is clearly seen by comparing results for LSi and HSi alloys. In contrast, comparing data

Table 2. Chemical composition measured on the keel blocks and calculated *CE* values (see text).

Reference	mass%							
	C	Si	*CE**	*CE***	Mn	P	S	Cr
LSi-RE-FE	3.53	2.43	4.21	4.29	0.17	<0.015	0.008	0.03
LSi-RE-FERE	3.46	2.48	4.15	4.24	0.17	<0.015	0.009	0.03
LSi-NRE-FE	3.65	2.23	4.27	4.35	0.15	0.017	0.011	0.03
HSi-RE-FE	3.28	3.70	4.32	4.43	0.19	<0.015	0.006	0.03
HSi-RE-FERE	3.29	3.82	4.36	4.48	0.18	<0.015	0.008	0.03
HSi-NRE-FE	3.29	3.49	4.27	4.38	0.17	0.018	0.011	0.04
HSiHC-RE-FE	3.43	3.70	4.47	4.59	0.17	<0.015	0.008	0.03
HSiHC-RE-FERE	3.35	3.90	4.44	4.57	0.19	<0.015	0.008	0.03
HSiHC-NRE-FE	3.55	3.46	4.52	4.63	0.18	0.018	0.011	0.04
Reference	Ni	Cu	Ti	Mg	Ce	La	Sb	
LSi-RE-FE	0.03	0.05	0.018	0.044	0.0051	0.0028	<0.0005	
LSi-RE-FERE	0.03	0.05	0.016	0.042	0.0046	0.0024	0.0007	
LSi-NRE-FE	0.03	0.06	0.021	0.038	<0.0005	<0.0005	<0.0005	
HSi-RE-FE	0.03	0.05	0.018	0.039	0.0042	0.0021	<0.0005	
HSi-RE-FERE	0.02	0.04	0.021	0.041	0.0041	0.0020	<0.0005	
HSi-NRE-FE	0.03	0.05	0.021	0.038	<0.0005	<0.0005	<0.0005	
HSiHC-RE-FE	0.10	0.06	0.021	0.037	0.0045	0.0021	<0.0005	
HSiHC-RE-FERE	0.09	0.08	0.027	0.036	0.0045	0.0021	<0.0005	
HSiHC-NRE-FE	0.05	0.05	0.022	0.040	<0.0005	<0.0005	<0.0005	

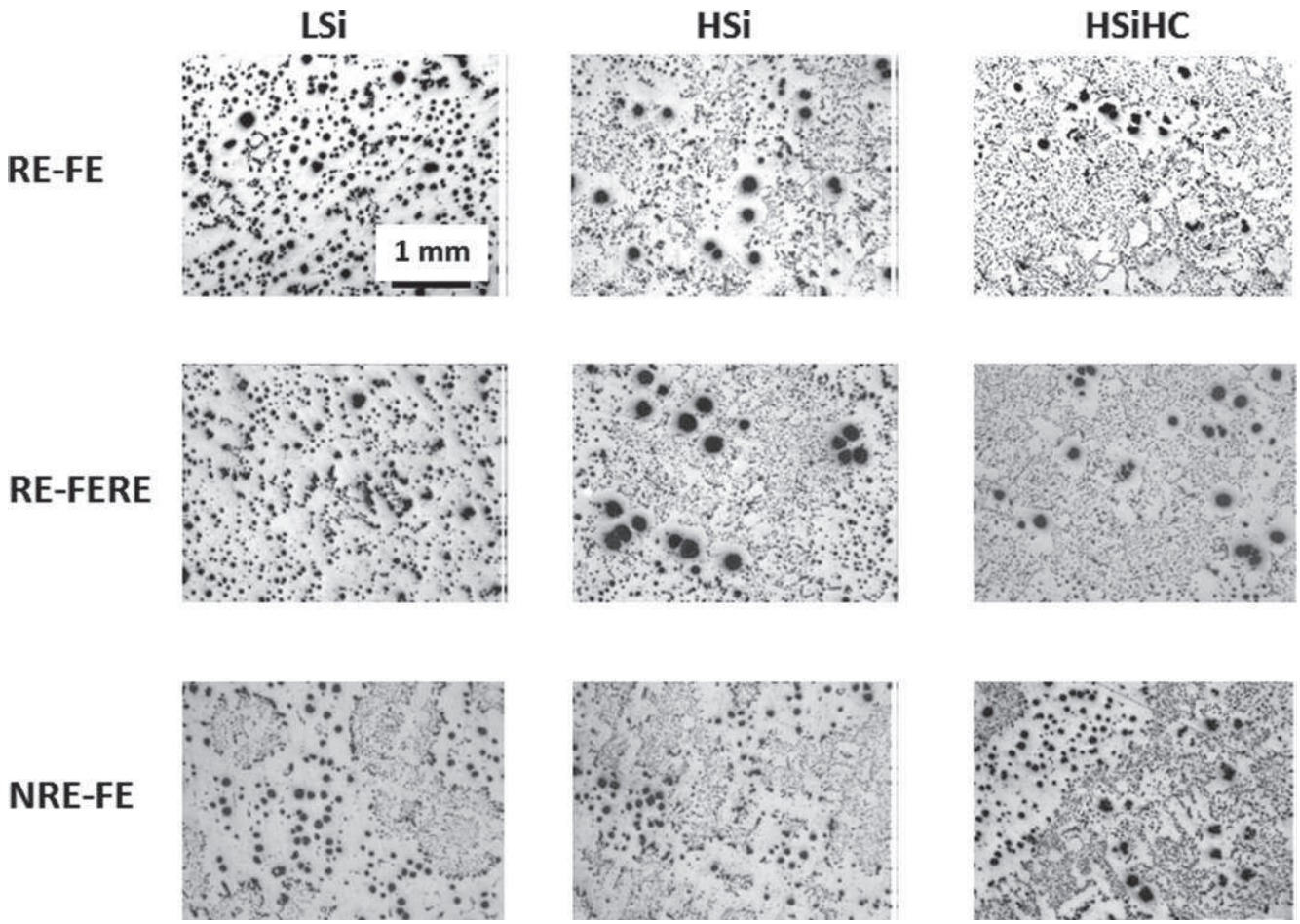

Fig. 3. Typical micrographs from the central part of Y4 blocks. All micrographs are at the same scale shown in the top left image.

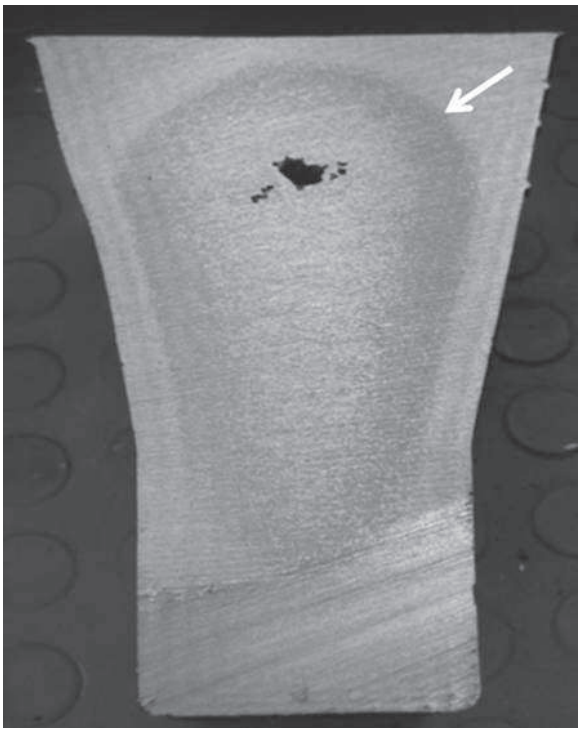

Fig. 4. Section of a Y3 keel-block showing the abrupt change in contrast (white arrow) associated with appearance of chunky graphite. The bottom thickness of the keel-block is 50 mm.

for HSi and HSiHC, it is seen that there is hardly any effect of carbon equivalent.

For checking any effect of inoculation efficiency, the nodule count measured at the bottom of the Y2 keel-blocks where chunky graphite never appeared are indicated by numbers in Fig. 5. If higher nodule count is associated with higher chunky fraction in the case of NRE-FE and RE-FERE alloys, the opposite is seen for RE-FE alloys. From this series of experiments, it seems that no conclusion could be drawn for nodule count effect on chunky graphite formation, in contradistinction with previous works where the

Table 3. Surface fraction of the observed sections affected by chunky graphite (%).

Reference	Y4	Y3	Y2
LSi-RE-FE	0	0	0
LSi-RE-FERE	0	0	0
LSi-NRE-FE	45	35	0
HSi-RE-FE	41	27	0
HSi-RE-FERE	26	15	0
HSi-NRE-FE	69	48	21
HSiHC-RE-FE	29	31	0
HSiHC-RE-FERE	18	11	0
HSiHC-NRE-FE	74	56	25

effect of melt inoculation on chunky graphite was studied [20].

Finally, the most evident result is the positive effect of RE addition on decreasing the amount of chunky graphite. As a matter of fact, the highest chunky fractions were found in the case of NRE-FE alloys for all three types of alloy compositions, that is when no RE was added to the melt. This is further illustrated with Fig. 6 where f_{CHG} has been plotted versus the cerium content for the three types of keel-blocks investigated in the present work.

This observation apparently contradicts the generally accepted view that RE favors the formation of chunky graphite. It should be stressed however that the amount of residual RE in the present alloys is very low as appearing in Fig. 6. The present observation then agrees with the review by Hoover [21] and results reported by Beers [22], though in this latter case cerium was added together with bismuth

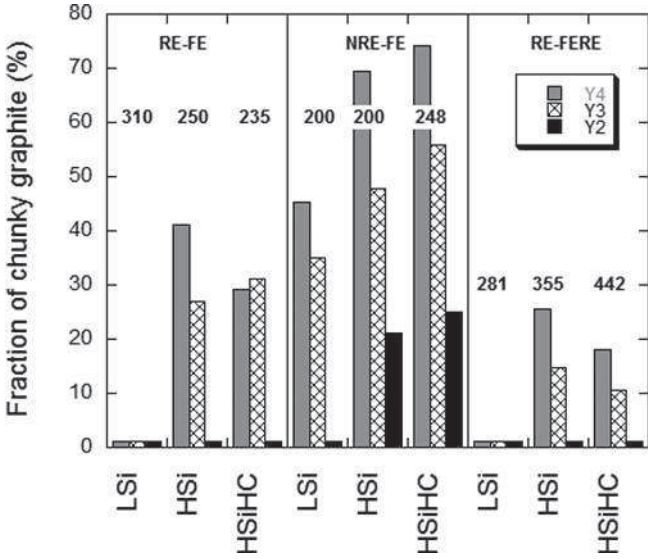

Fig. 5. Effect of silicon and carbon contents on chunky graphite amount. Numbers are nodule counts (mm^{-2}) measured at the bottom of Y2 blocks.

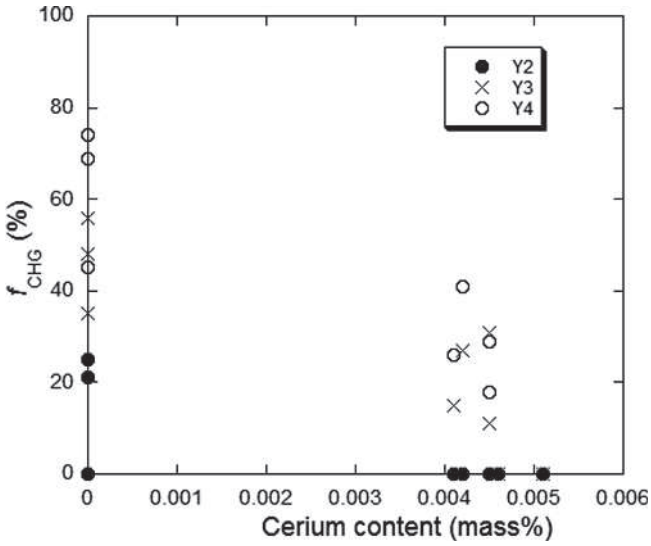

Fig. 6. Effect of cerium addition on the amount of chunky graphite as observed in the present study.

which is a so-called anti-nodularizing element. This may also be linked to the beneficial effect of low level RE on nodularity as shown by White et al. [1]. In fact, Skaland [23] has reviewed a number of works showing there is an optimum RE content for either graphite nodularity or nodule count. This optimum was seen to change from one work to another, thus being highly sensitive to base metal composition or processing variable [23].

For checking if such an optimum amount of cerium or RE exists also for chunky graphite appearance, the present results were compared with previous work when Y2 keel-blocks were used [24]. A general trend is obtained for this casting size with a minimum area affected by chunky graphite for a cerium content of 0.004–0.005 mass%. Such a value is in the low range of the optimum values reported by Skaland [23], and would further decrease with increase in the casting section size.

4. Discussion

Following Mampaey [25], it is expected that the eutectic reaction in ductile iron heavy section castings takes place after the development of a network of austenite dendrites with the mushy eutectic zone occupying a large part of the cast component. Accordingly, it has been observed that in a cubic block 500 mm in size which solidifies in 3.5 h, the temperature is homogeneous after less than 30 min and the eutectic reaction takes place at the same temperature in most of the block [5]. In other words, the temperature at which the eutectic reaction starts close to the surface of the casting imposes the minimum temperature at which the eutectic reaction proceeds in locations remote from the surface. This suggested investigating if the change in the growth rate of austenite dendrites from the surface to the center of the casting could affect to any extent redistribution of solutes and thus could change the conditions under which the eutectic reaction initiates. Calculations described in Appendix 1 show that there is no effect of cerium at the level added and no significant change in the relation between growth rate and undercooling of austenite when changing the carbon and silicon contents in the range investigated.

However, silicon does segregate negatively, thus accumulating in austenite, which means that the liquid ahead of the austenite/melt interface gets impoverished in this element. Further, as the eutectic temperature decreases with lowering the silicon content, silicon redistribution between austenite and liquid leads to a slightly lower eutectic undercooling at the austenite/liquid interface as compared to bulk liquid. Such a situation of low eutectic undercooling has been suggested to favor chunky graphite formation [8, 26] and this could possibly explain the role of increased silicon content observed experimentally in the present work. The same argument could as well explain the detrimental effect of aluminum on graphite nodularity (see for example Hecht and Nonon [27]) as the Fe–C–Al system presents a strong similarity to the Fe–C–Si system.

Because chunky graphite is recognized as resulting from a coupled growth of austenite and graphite, it seemed of interest to consider the conditions needed for such growth to take place. The discussion will be based on surface energy values from McSwain et al. [28] which are shown in Fig. 7 though other literature data are reviewed in appendix 2. It

is seen in Fig. 7 that the interfacial energy between prismatic graphite planes and liquid $\gamma^{l/Gp}$ is less than 0.70 times that of the basal planes $\gamma^{l/Gb}$ for sulfur-bearing alloys, i.e. alloys which have not been nodularized. Magnesium- or cerium-treated alloys show a reverse trend, with $\gamma^{l/Gb}$ being smaller than $\gamma^{l/Gp}$ in a ratio of 0.85–0.90 [28].

Before dealing with coupled growth, it is interesting to consider the consequences of Fig. 7 on primary graphite growth. In untreated alloys, graphite grows along the prism direction and develops large basal facets. However, the growing edges do not show prism $(01\bar{1}0)$ facets but rather facets with intermediate orientations or even a rounded shape similar to that of a rough interface [29]. Accordingly, there should be a cusp in the angular plot of $\gamma^{l/G}$ for the basal orientation and maybe simply a rounded minimum for the prism orientation. The evolution of $\gamma^{l/G}$ in the $(\bar{1}\bar{1}20)$ plane from the $[0001]$ direction to the $[1\bar{1}00]$ direction has been tentatively represented with solid lines in Fig. 7 for both untreated and nodularized alloys. Intermediate cusps may exist corresponding to facets with intermediate orientations, but there is no need to consider them here. According to data in Fig. 7, the stable shape of graphite in untreated cast irons should be a pyramid with an axis parallel to the basal direction and with a hexagonal section, thus quite similar to the highly crystalline graphite crystal pyramids from Sterling Hill [30].

That primary graphite in untreated alloys develops as plates or lamellas and not as pyramids during cast iron solidification clearly indicates the evolving microstructure is controlled by growth kinetics. In the case of nodularized alloys where $\gamma^{l/Gb}$ is slightly lower than $\gamma^{l/Gp}$, Selçuk and Kirkwood [31] could state: "it is readily appreciated that a spherulite is thermodynamically favoured since it is bounded by the lowest energy faces". Following the lines proposed by Fullman [32], this statement has been refined by Takita and Ueda [33] who compared the total interfacial energy of a plate-like hexagonal single crystal and that of a spherulite made of 400 radial sectors for explaining shape change.

Coupled growth needs mechanical equilibrium to be established at the tri-junction between liquid, austenite and graphite. This equilibrium follows the Young–Herring equation [34]:

$$\gamma^{l/G}\cdot\boldsymbol{t}^{l/G}-(\gamma^{l/G})'\cdot\boldsymbol{n}^{l/G}+\gamma^{l/\gamma}\cdot\boldsymbol{t}^{l/\gamma}-(\gamma^{l/\gamma})'\cdot\boldsymbol{n}^{l/\gamma}+\gamma^{\gamma/G}\cdot\boldsymbol{t}^{\gamma/G}-(\gamma^{\gamma/G})'\cdot\boldsymbol{n}^{\gamma/G}=0 \quad (1)$$

where the $\boldsymbol{t}$ and $\boldsymbol{n}$ are the tangential and normal interface vectors, while the prime denotes the derivative with respect to rotation angle, i.e. characterizes the angular dependence of the surface energy of a given interface. This normal component is called torque, it acts on the interface to drive it towards the nearest (local) minimum of the interfacial energy.

The anisotropy of the austenite/liquid interface is certainly very small and can be neglected, and it will be assumed this applies as well to the austenite/graphite interface. This latter assumption is known to be wrong in some systems where the anisotropy of the solid/solid interface energy leads to lamellar drift during eutectic growth [35]. However, in the case of cast irons, the fact that compact graphite can be grown directionally and show random orientation [36] is a strong indication that austenite/graphite interface energy does not significantly vary with the relative orientation of the phases. Accordingly, the Young–Herring Eq. (1) then simplifies to:

$$\gamma^{l/G}\cdot\boldsymbol{t}^{l/G}-(\gamma^{l/G})'\cdot\boldsymbol{n}^{l/G}+\gamma^{l/\gamma}\cdot\boldsymbol{t}^{l/\gamma}+\gamma^{\gamma/G}\cdot\boldsymbol{t}^{\gamma/G}=0 \quad (1')$$

According to the data assessed in the work by Sayama et al. [37], $\gamma^{\gamma/G}$ is of the order of $0.9-1\ \mathrm{J\cdot m^{-2}}$ and is thus slightly lower than $\gamma^{l/Gp}$ for untreated alloys, while $\gamma^{l/\gamma}$ is much lower at about $0.2-0.3\ \mathrm{J\cdot m^{-2}}$. It is further expected that $\gamma^{l/\gamma}$ and $\gamma^{\gamma/G}$ are not strongly sensitive to chemistry changes and will accordingly be taken as constant in all the following.

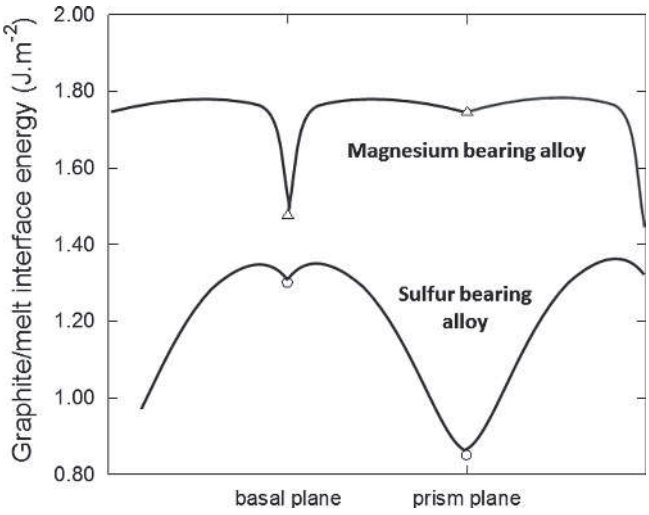

Fig. 7. Graphite/melt interfacial energy: symbols are experimental values according to McSwain et al. [28], lines are tentative evolution in the $(\bar{1}\bar{1}20)$ plane.

Figure 8a illustrates the case of coupled growth of austenite and lamellar graphite during which this latter grows along the prism direction while developing large basal facets behind the solidification front. The graphite surface is shown rounded which may represent vicinal faces and correspond to a value of $\gamma^{l/G}$ intermediate between $\gamma^{l/Gp}$ and $\gamma^{l/Gb}$, see Fig. 7. The torque tends to rotate the graphite/liquid interface towards the prism direction and has been drawn accordingly. Austenite curvature is shown convex towards the liquid at the triple junction and must change at some distance from it for the eutectic front to remain nearly isothermal.

In Fig. 8a, the thin lines show the sum of the first two terms in Eq. (1′), $\boldsymbol{\sigma}$, and of the last two terms, $\boldsymbol{S}$. Their length is such that the balance of force is nearly but not satisfied. One possibility which makes the mechanical equilibrium at the triple junction to be more easily satisfied is illustrated in Fig. 8b where the curvature of austenite has been reversed. Thus, the shape of graphite in contact with the liquid and austenite curvature at the triple junction depend on $\gamma^{l/G}$ which may be affected in particular by the oxygen and sulfur content of the melt. In case of increased oxygen and sulfur contents, $\gamma^{l/G}$ decreases making easier the achievement of the Young–Herring condition. On the opposite, one may imagine that the amount of oxygen and sulfur in the liquid could decrease with time. In such a case, $\gamma^{l/Gp}$

increases and so must do the actual $\gamma^{l/G}$ value. This would lead to an unstable triple-junction and austenite will show a tendency to envelop graphite [38]. This is the case of nodularized melts for which Eq. (1′) cannot be satisfied with the configurations shown in Fig. 8a or b. Accordingly, the nodularizing treatment may be seen as basically related to a change in melt chemistry that forbids coupled growth of austenite and graphite if this latter was to grow along its prismatic direction.

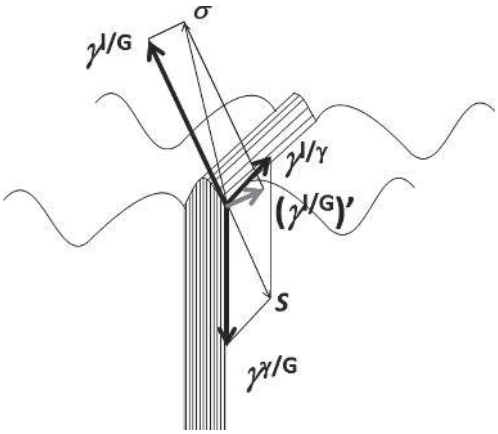

(a)

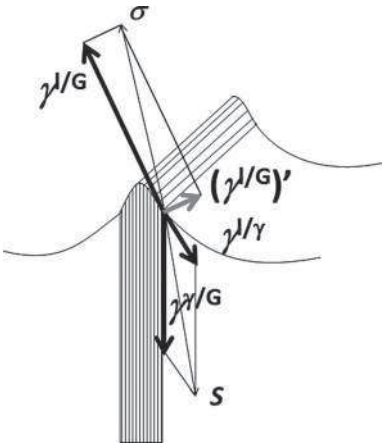

(b)

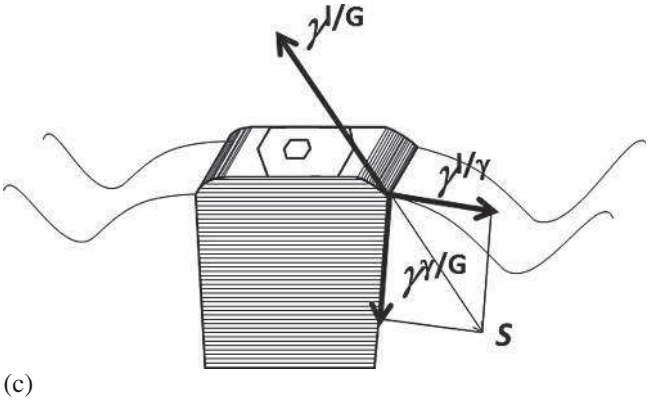

(c)

Fig. 8. Schematic of coupled growth of graphite when: (a) graphite grows along the prismatic direction with positive curvature of austenite at the triple junction; (b) graphite grows along the prismatic direction with negative curvature of austenite at the triple junction; and (c) graphite grows along the basal direction with positive curvature of austenite at the triple junction. The forces acting at the triple junction are shown in bold lines, their (near) equilibrium is illustrated with the thin lines.

Let us now consider that the melt has been modified so that the overall (or apparent) growth direction of graphite is the ***c*** direction. Though it is accepted that cells of chunky graphite do grow in some coupled way, details of the liquid/eutectic interface and growth mechanism are unknown. A simplified schematic of the interface is anyway proposed in Fig. 8c where basal planes of graphite are now in contact with the liquid but where steps and intermediate facets develop on the edges of graphite. According to the orientation change in $\gamma^{l/G}$ proposed in Fig. 7 for nodularized alloys, the torque at the triple junction may then be very low and could be neglected. With the value of $\gamma^{l/G}$ at 1.5 – 1.7 J · m^{-2} and the same values as above for the other interfacial energies, it is seen in Fig. 8c that the balance of forces is not satisfied, with $|\boldsymbol{S}| < \gamma^{l/G}$. However, a slight over treatment of the melt in Mg and/or Ce, or the accumulation at the graphite/liquid interface of other surface active elements, may easily decrease $\gamma^{l/G}$ below a critical value of about 1.3 J · m^{-2} where the balance of forces could be achieved.

The above considerations suggest that low additions of cerium and RE as in the present work increase $\gamma^{l/Gb}$ by further deoxidizing and desulfurizing the melt and thus decrease the risk of chunky graphite formation as observed. However, higher additions of RE, once the melt is totally deoxidized and desulfurized, would then lead to a significant decrease in $\gamma^{l/Gb}$ and to the potential formation of chunky graphite. This latter condition corresponds to the so-called RE over treatment in the case of heavy section castings.

Figure 8c further suggests that overall growth of graphite along the ***c*** direction proceeds by nucleation and growth of new layers on top of the basal surface, and their growth by lateral spreading. Such a process has been previously considered in a simple approach of exploded graphite formation [39] and for describing thickening of graphite lamellas [29].

5. Conclusion

Dedicated experiments were carried out that showed chunky graphite formation in nodular cast iron:

- Decreases with increase in cooling rate and with low-level addition of RE;
- Increases with increase in alloy silicon content;
- Is not sensitive to carbon equivalent.

By considering conditions for coupled growth of graphite and austenite, a schematic could be proposed which shows that chunky graphite would be favored in the case of too-high level of surface active elements and in particular of nodularizers (Mg and RE). This schematic also suggests that the nodularizing treatment may be seen as basically related to a change in melt chemistry that forbids coupled growth of austenite and graphite.

Discussion with as well as criticism from S. Akamatsu and J. Eiken are deeply acknowledged.

References

[1] C.V. White, R.A. Flinn, P.K. Trojan: AFS Trans. 91 (1983) 549.
[2] T. Thielemann: GiessereiTechnik 16 (1970) 16.
[3] B. Lux: AFS Cast Met. Res. J. 8 (1972) 25.
[4] O. Tsumura, Y. Ichinomiya, H. Narita, T. Miyamoto, T. Takenouchi: IMONO 67 (1995) 540.

[5] P. Larranaga, I. Asenjo, J. Sertucha, R. Suarez, I. Ferrer, J. Lacaze: Metall. Mater. Trans. 40A (2009) 654. DOI:10.1007/s11661-008-9731-y
[6] P.C. Liu, C.L. Li, D.H. Wu, C.R. Loper: AFS Trans. 91 (1983) 119.
[7] H. Itofuji, H. Uchikawa: AFS Trans. 98 (1990) 429.
[8] J. Lacaze, L. Magnusson-Åberg, J. Sertucha: Proc. Keith Millis symposium, Nashville, AFS, (2013) 232.
[9] S.I. Karsay, E. Campomanes: AFS Trans. 78 (1970) 85.
[10] B. Prinz, K.J. Eschborn, T. Schulze, R. Döpp, E. Schurmann: Giessereiforschung 43 (1991) 107.
[11] T.C. Xi, J. Fargues, M. Hecht, J.C. Margerie: Mat. Res. Soc. Symp. Proc. 34 (1985) 67. DOI:10.1557/PROC-34-67
[12] K. Hamberg, L.E. Björkgren, Z.X. Sun: Svenska Gjuteriföreningen (1997) 16.
[13] H. Löblich: Giesserei 93 (2006) 28.
[14] W. Stets, U. Petzschmann, R. Hentsch, A. Lötschert: Giesserei 101 (2014) 36.
[15] M. Gagné, D. Argo: Proc. of Advanced casting technology, ASM Int. (1987) 231.
[16] M. Castro, M. Herrera, M.M. Cisneros, G. Lesoult, J. Lacaze. Int. J. Cast Met. Res. 11 (1999) 369.
[17] D.M. Stefanescu, J. Lacaze: ASM Handbook, Volume 1A, Cast Irons, in press.
[18] R. Källborn, K. Hamberg, M. Wessén, L.E. Björkegren: Mater. Sci. Eng. A 413–414 (2005) 346. DOI:10.1016/j.msea.2005.08.210
[19] X.G. Diao, Z.L. Ning, F.Y. Ren, J.F. Sun: Mater. Sci. Technol. 27 (2011) 834. DOI:10.1179/026708309X12560332736557
[20] I. Asenjo, P. Larranaga, J. Sertucha, J. Sertucha, R. Suarez, J.M. Gomez, I. Ferrer, J. Lacaze: Int. J. Cast Met. Res. 20 (2007) 319. DOI:10.1179/136404608X286138
[21] H.W. Hoover: AFS Trans. 94 (1986) 601.
[22] M. Beers: 117th Metalcasting Congress, AFS (2013), paper 13–1236.
[23] T. Skaland: Proc. AFS Cast Iron Inoculation Conf. (2005), 13.
[24] I. Asenjo, J. Lacaze, P. Larranaga, S. Méndez, J. Sertucha, R. Suarez: Key Eng. Mater. 457 (2011) 52. DOI:10.4028/www.scientific.net/KEM.457.52
[25] F. Mampaey: AFS Trans. 107 (1999) 425.
[26] J. Sertucha, R. Suarez, I. Asenjo, P. Larranaga, J. Lacaze, I. Ferrer, S. Armendariz: ISIJ Int. 49 (2009) 220. DOI:10.2355/isijinternational.49.220
[27] M. Hecht, E. Nonon: Int. J. Met. Cast. Res. 16 (2003) 307. DOI:10.1179/136404603225007061
[28] R.H. McSwain, C.E. Bates, W.D. Scott: AFS Cast Met. Res. J. 10 (1974) 181.
[29] S. Amini, R. Abbaschian: Carbon 51 (2013) 110. DOI:10.1016/j.carbon.2012.08.019
[30] J.A. Jaszczak: The Picking Table 35 (1994) 6.
[31] E. Selçuk, D.H. Kirkwood: J. Iron Steel Inst. February issue (1973) 134.
[32] R.L. Fullman: Acta Metall. 5 (1957) 638. DOI:10.1016/0001-6160(57)90110-4
[33] M. Takita, Y. Ueda: Trans. Japan Inst. Met. 20 (1979) 569. DOI:10.2320/matertrans1960.20.569
[34] D.W. Hoffman, J.W. Cahn: Surf. Sci. 31 (1974) 368. DOI:10.1016/0039-6028(72)90268-3
[35] S. Akamatsu, S. Bottin-Rousseau, M. Serefoglu, G. Faivre: Acta Mater. 60 (2012) 3199. DOI:10.1016/j.actamat.2012.02.031
[36] A. Roviglione, J.D. Hermida: Mater. Charact. 32 (1994) 127. DOI:10.1016/1044-5803(94)90099-x
[37] Y. Sayama, T. Sato, G. Ohira: J. Cryst. Growth 22 (1974) 272. DOI:10.1016/0022-0248(74)90171-7
[38] M. Hillert: Jernkont. Ann. 141 (1957) 53.
[39] R. Ghergu, L. Magusson-Aberg, J. Lacaze: Mater. Sci. Forum 790–791 (2014) 435. DOI:10.4028/www.scientific.net/MSF.790–791.435
[40] M. Bobadilla, J. Lacaze, G. Lesoult : J. Cryst. Growth 89 (1988) 531. DOI:10.1016/0022-0248(88)90216-3
[41] N. Siredey, J. Lacaze: Scr. Metall. Mater. 29 (1993) 759. DOI:10.1016/0956-716X(93)90222-E
[42] Xuping Su, J.C. Tedenac: Calphad 30 (2006) 455. DOI:10.1016/j.calphad.2006.06.003
[43] C. Selig, J. Lacaze: Metall. Mater. Trans. B 31 (2000) 827. DOI:10.1007/511663-000-0119-7
[44] B.S. Mil'man, N.N. Aleksandrov, V.T. Solenkov, L.V. Il'cheva: Russian casting production 5 (1976) 179.
[45] H.T. Angus: Cast iron: Physical properties and engineering properties, Butterworths, (1975) 123.
[46] Y. Ueda, M. Takida, Zeng Da-Ben, T. Kishi: Trans. Japan Inst. Met. 27 (1986) 70. DOI:10.2320/matertrans1960.27.70

(Received June 7, 2016; accepted August 26, 2016; online since September 29, 2016)

Correspondence address

Jacques Lacaze
CIRIMAT
Université de Toulouse
ENSIACET
4 rue Monso
CS 44362
Toulouse 31030
France
Tel.: +33-5-34-32-34-15
Fax: +33-5-34-32-33-99
E-mail: Jacques.lacaze@ensiacet.fr
Web: http://cirimat.cnrs.fr/

Appendix 1

Calculation of solute redistribution at the tip of austenite dendrites has been performed using an approach for multicomponent alloys previously described [40, 41]. Calculations were achieved considering carbon, silicon and cerium as alloying elements. From the thermodynamic assessment of the Fe–Ce system carried out by Su and Tedenac [42], the Ce partition coefficient between austenite and liquid, $k_{\mathrm{Ce}}^{\gamma/\mathrm{l}}$, and the slope of the austenite liquidus, $m_{\mathrm{Ce}}^{\mathrm{l}/\gamma}$, were evaluated at 0.002 and –15.2 °C/mass% respectively. Data for carbon and silicon were taken from a previous work on microsegregation in cast irons [43]:

$$k_{\mathrm{C}}^{\gamma/\mathrm{l}} = 0.47$$

$$k_{\mathrm{Si}}^{\gamma/\mathrm{l}} = 1 + 0.0067 \cdot (1200 - T) \cdot \left(1 - \frac{w_{\mathrm{Si}}}{0.07}\right)$$

$$T_{\mathrm{L}}^{\gamma} = 1567.3 - 97.3 \cdot \mathrm{w_C} - 23.0 \cdot w_{\mathrm{Si}}$$

where w_{Si} and w_{C} are the mass fraction (%) of carbon and silicon in the alloy, T and T_L^{γ} are the temperature of the alloy and the austenite liquidus temperature respectively (°C). The diffusion coefficients in the liquid were set to $5 \cdot 10^{-9}\ \mathrm{m^2\,s^{-1}}$ for carbon and $10^{-9}\ \mathrm{m^2\,s^{-1}}$ for silicon and cerium.

With the data above, it has been observed that the effect of cerium is negligible at the level it has been added. Accordingly, only redistribution of carbon and silicon was

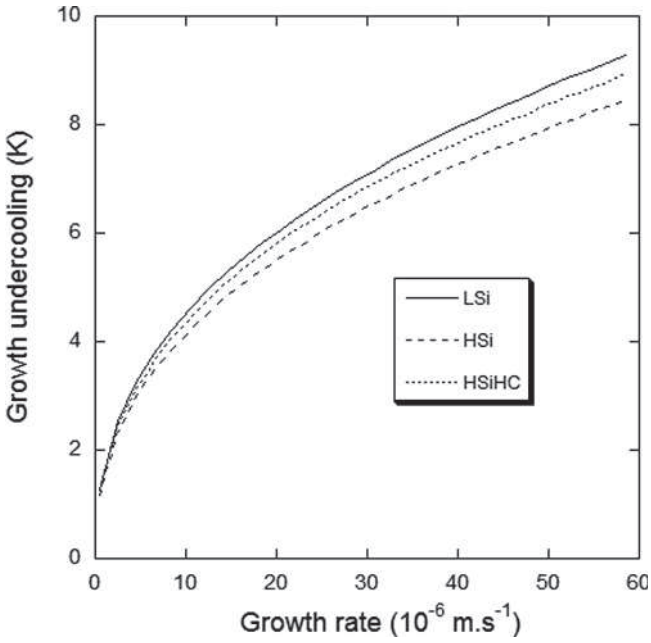

Figure A1. Evolution of the dendrite tip growth undercooling with the growth rate for Fe–C–Si alloys with compositions corresponding to LSi, HSi and HSiHC alloys.

considered for further calculations. Figure A1 shows the evolution of the austenite growth undercooling with the growth rate. From the outer surface to the middle of the casting, the growth rate is expected to decrease and it is seen that the growth undercooling decreases to quite a low value. Further, it is observed that increasing silicon content leads to a lower undercooling at a given growth rate, though this effect is quite limited.

Appendix 2 – Graphite/melt interfacial energy

As a general rule, interfacial energy measurement is difficult because it may depend on a large number of experimental parameters. Though other means are available such as measurement of the bubbling pressure of a gas or change in shape of a levitated droplet, the most common way of measuring the surface tension of a liquid, γ^{l}, is by looking at the stationary shape of a melt droplet deposited on a non-reactive substrate (the sessile drop technique). If the substrate is made of graphite, measuring the contact angle of the drop with the substrate further gives an estimate of $(\gamma^{l/G} - \gamma^{G})$ with $\gamma^{l/G}$ being the interfacial energy between graphite and liquid and γ^{G} the surface energy of graphite. The above difference has been called the relative surface energy by Selçuk and Kirkwood [31].

The surface tension γ^{l} has often been used to correlate cast iron melt properties with graphite shape in as-cast alloys [28], but Mil'man et al. [44] demonstrated experimentally that the evolution of the relative surface energy with alloying may not always parallel that of the surface energy. McSwain et al. [28] reviewed the work done before 1974 and made clear that addition of any trace or common alloying elements does decrease the surface tension of the melt. Accordingly, the increase associated with addition of deoxidizers and desulfurizers such as Mg and Ce to a standard iron is due to the removal of the free O and S from the melt, and this has been stressed again by Angus [45]. Further addition of these elements after complete removal of O and S decreases the surface tension.

One of the main difficulties with cast iron is that strong surface active elements such as oxygen, sulfur, magnesium and cerium are quite volatile as well. This means that the value of the surface tension and of the contact angle may evolve during experiments. The most precise data on this evolution are due to Selçuk and Kirkwood [31] who correlated the change with time of the droplet shape and of the relative surface energy with the loss in either Mg, Ce or S which were the alloying elements considered in their experiments. Their experiments were performed at 1200 °C under secondary vacuum with a substrate made of pure graphite (assumed polycrystalline). As expected, the authors found that the significant increase in the surface energy of the S-bearing melt during holding at 1200 °C correlates with a parallel decrease in the S content of the alloy. In contrast, it was found that the surface tension of the melt and the relative interface energy did decrease with time for Mg- and Ce-bearing alloys whilst the content of these elements was decreasing with time. This behavior is explained by the authors as being due to the loss of either Mg or Ce, which led to a release in the melt of sulfur that was tight in sulfides of these elements.

A further step was achieved by McSwain et al. [28] by using various kinds of graphite as substrate, namely basal- and prism-oriented pyrolytic graphite and polycrystalline graphite that has a mixed orientation. The authors considered values of γ^{G} from literature (1.096 J · m^{-2} and 0.983 J · m^{-2} for prism and basal planes respectively) so that $\gamma^{l/G}$ could be evaluated. Melting of magnesium-bearing, cerium-bearing and sulfur-bearing alloys was achieved under nitrogen and measurement performed at 1200 °C. These results appear consistent and have been used in the main text of the present work. The definite conclusion drawn by the authors when looking at the microstructure of the drops after solidification is that the graphite shape relates to growth along the pole having the lowest interfacial energy.

Mil'man et al. [44] used a substrate made of "pseudo-single-crystal" oriented along the prismatic or basal planes of graphite. Measurements were achieved under argon at 1300 °C with alloys prepared from pure components. The authors considered that γ^{G} was constant but its value was not specified. The effect of Mg, Ce, Bi, Sb and Sn was investigated and it was found that the interfacial energy of prism and basal planes evolves with holding time as reported by Selçuk and Kirkwood [31]. From all their measurements, they could conclude that for nodular graphite to appear not only should the interface energy $\gamma^{l/Gb}$ of the basal planes be lower than $\gamma^{l/Gp}$ for prism planes, but it should also achieve a high enough value of at least 1.15 J · m^{-2}. All values reported by Mil'man et al. [44] for alloys showing nodular graphite after experiment are close to those of McSwain et al. [28] being between 1.20 and 1.24 J · m^{-2} for basal planes and between 1.27 and 1.39 J · m^{-2} for prism planes. Values for samples with flake graphite could be less than 0.2 J · m^{-2} in the case of high oxygen level (35 ppm) but were generally in the range 0.8 to 1.0 J · m^{-2}.

Takita and Ueda [33] and Ueda et al. [46] conducted similar experiments to investigate the effect of magnesium and cerium, respectively. The former experiments were per-

formed at 1180 °C and the latter at 1190 °C. The substrate was either polycrystalline or pyrolytic graphite. In both cases it was found that the measurements evolved during the 30 min holding, and the authors chose to use the average of three measurements made at the beginning of the holding. The results on Mg show a consistent decrease of $\gamma^{I/Gb}$ with increase in the magnesium content with a value that agrees with that of McSwain et al. [28] for similar composition. The corresponding values for the prism planes show little effect of the magnesium content. The results for the effect of cerium show little effect of increasing the cerium content on the basal plane while a significant increase is seen for the prism plane.

In all the works reviewed above, care was generally taken to use hypereutectic alloys to avoid reaction between the iron melt and graphite substrate. Conversely, this may explain why no data have been found concerning the most important elements, namely carbon and silicon.